# Galaxy Colour, Morphology, and Environment in the Sloan Digital Sky Survey

N. M. Ball,  $^{1,2\star}$  J. Loveday<sup>3</sup> and R. J. Brunner<sup>1,2</sup>

- <sup>1</sup>Department of Astronomy, MC-221, University of Illinois, 1002 West Green Street, Urbana, IL 61801, USA
- <sup>2</sup> National Center for Supercomputing Applications, MC-476, University of Illinois, 605 East Springfield Avenue, Champaign, IL 61820, USA

Accepted xxxx Received xxxx

## ABSTRACT

We use the Fourth Data Release of the Sloan Digital Sky Survey to investigate the relation between galaxy rest frame u-r colour, morphology, as described by the concentration and Sérsic indices, and environmental density, for a sample of 79,553 galaxies at  $z \lesssim 0.1$ . We split the samples according to density and luminosity and recover the expected bimodal distribution in the colour-morphology plane, shown especially clearly by this subsampling.

We quantify the bimodality by a sum of two Gaussians on the colour and morphology axes and show that, for the red/early-type population both colour and morphology do not change significantly as a function of density. For the blue/late-type population, with increasing density the colour becomes redder but the morphology again does not change significantly. Both populations become monotonically redder and of earlier type with increasing luminosity. There is no significant qualitative difference between the behaviour of the two morphological measures.

Motivated by their long-standing use in astronomy and their ability to utilise information not necessarily used by the concentration and Sérsic indices, we supplement the morphological sample with 13,655 galaxies assigned Hubble types by an artificial neural network. We find, however, that the resulting distribution is less well described by two Gaussians. Therefore, there are either more than two significant morphological populations, physical processes not seen in colour space, or the Hubble type, particularly the different subtypes of spirals Sa–Sd, has an irreducible fuzziness when related to environmental density.

For each of the three measures of morphology, on removing the density relation due to it, we recover a strong residual relation in colour. However, on similarly removing the colour-density relation there is no evidence for a residual relation due to morphology. Therefore, either the morphology is not directly affected by the environmental density beyond the correlation to colour, or a single galaxy 'type' does not capture sufficient information.

**Key words:** cosmology: observations – methods: data analysis – methods: statistical – galaxies: fundamental parameters – galaxies: statistics

## 1 INTRODUCTION

The connection between the morphology of a galaxy and the density of its environment (e.g. Oemler 1974; Dressler 1980), measured in a variety of ways, is an important clue to the physics of galaxy formation, and forms a readily observable quantity that can be compared with simulations.

Numerous physical processes affect the evolution of a galaxy as a function of its density environment. The debate is ongoing as to which of these are intrinsic to the galaxies at formation and which are the result of later evolution. The relative importance of different processes depends on the density of the environment. For example,

\* E-mail: nball@astro.uiuc.edu

in clusters infalling galaxies are subject to ram-pressure stripping and galaxy harassment. In groups, mergers, interactions and strangulation are more important. It is thought that ellipticals formed their stars early, exhausting their gas supply and are now passively evolving in dense environments, whereas spirals formed their stars more slowly, continuing to the present day and becoming subject to the physical processes described on infall into denser environments as the structure evolved. We do not attempt to provide a full reference list for physical processes here, but recent reviews of the subject include Boselli & Gavazzi (2006), Hogg (2006) and Avila-Reese (2007).

However, the morphology of the galaxies is affected in ways not necessarily correlated with the effect on spectral properties or colour. One can therefore investigate the morphology-density and

<sup>&</sup>lt;sup>3</sup>Astronomy Centre, University of Sussex, Falmer, Brighton, BN1 9QJ, UK

colour-density relations and subtract the two to see if a residual relation remains. If so, then there is an intrinsic effect of density that is not a result of a more fundamental process which causes the other relation.

A particular example of this is the hypothesis that the properties of galaxies within a dark matter halo depend only on the mass of the halo (e.g. Cooray & Sheth 2002) This can be tested both for colour and for morphology, although here we do not specifically relate our results to haloes. Many results support this assumption (e.g. Blanton et al. 2006; Abbas & Sheth 2006; Blanton & Berlind 2007; Tinker et al. 2007).

Numerous existing results support colour as being a more fundamental predictor of environment than morphology (e.g. Kauffmann et al. 2004; Blanton et al. 2005b; Quintero et al. 2005; Martínez & Muriel 2006; Quintero et al. 2006). However, the question is not yet necessarily settled as Park et al. (2007) find that the morphology and luminosity are more fundamental. Similarly, Lane et al. (2007) study the Abell 901/902 supercluster and find that the local environment is more important than the global for morphology, but Einasto et al. (2007) study numerous superclusters in the 2dF Galaxy Redshift survey (Colless et al. 2001) and find that both the cluster and supercluster environment influence morphology.

An example of a physical process causing a distinct change in morphology is that of S0 galaxies. Christlein & Zabludoff (2004) find that they must have formed from bulge enhancement and not disc fading. Boselli & Gavazzi (2006) find that S0s are formed through gravitational interaction rather than spiral interaction with the intergalactic medium. Moran et al. (2007) directly image spirals in the process of being transformed into S0s.

In the SDSS, the colour-density relation was previously investigated by Balogh et al. (2004, hereafter B04). They found a pronounced bimodal distribution well-fit by a sum of two Gaussians. At fixed luminosity, the mean colours of the two distributions were approximately independent of environment, but the red fraction strongly increased with density. The density measure used was the projected distance to the fifth nearest neighbour in a redshift slice of width  $1000~{\rm km~s^{-1}}$ . The part of our work dealing with u-r significantly parallels this work, although for a sample size containing three times as many galaxies.

Previous work in the SDSS on the morphology-density relation includes Goto et al. (2003), in which they use the concentration index and the texture parameter of Yamauchi et al. (2005) to study galaxies in the SDSS Early Data Release (EDR, Stoughton et al. 2002). Sorrentino et al. (2006) use the u-r colour, the eClass eigenclass spectral type and the fraction of the galaxy profile described by a de Vaucouleurs profile (FracDeV) to describe their sample, with an emphasis on comparing galaxies in voids to the general population. Park et al. (2007) use an adaptive kernel estimate of density and the morphological separation via colour gradient of Park & Choi (2005) and find little residual dependence of properties on environment at fixed luminosity and morphology, except for a sharp decrease in late types at the bright end. Some of these results are described further in  $\S 3.5$  below.

Here, we use the Fourth Data Release (DR4, Adelman-McCarthy et al. 2006) of the Sloan Digital Sky Survey (SDSS, York et al. 2000) to investigate the colour-density and morphology-density relations in a large volume-limited sample. We divide the sample by density and luminosity and investigate the trends of colour and morphology as a function of each, fitting Gaussians to the bimodal distributions in colour and morphology.

The sample size, quality of photometry and corresponding

spectra enable robust conclusions to be drawn from the data. However, the available resolution limits us to simple measures of colour and morphology. Accordingly, as done by previous authors, we use the u-r colour, inverse concentration index,  $CI_{\rm inv}$  and the Sérsic index, n, each single-number axisymmetric measures of galaxy properties. However, in addition to this, we supplement the morphological measures with the Hubble type assigned by an artificial neural network (ANN, Ball et al. 2004). This assigns T types 0–6, corresponding to E, S0, Sa, Sb, Sc, Sd and Im, to a limiting magnitude of r < 15.9 (compared to r < 17.77 for u-r,  $CI_{\rm inv}$  and Sérsic n).

The Hubble type utilises more information from an image, for example spiral arm structure, and as such may show patterns unseen in the  $CI_{\rm inv}$  and Sérsic n. Given the wide usage over time of this measure (e.g. Sandage 2005) it is important that its usefulness is investigated in this context: if the results using the simple Hubble type used here are not useful even with the quality and quantity of the data we utilise, this will emphasize the requirement for different and more detailed measures of morphology for progress to be made.

This sample used here is the largest to date for which the Hubble type measure of morphology has been investigated as a function of environment (c.f. van den Bergh (2007), who use the detailed eyeball-assigned Hubble types for 1,246 galaxies from the Revised Shapley-Ames Catalogue (Sandage & Tammann 1981); and Conselice (2006), who construct a sample of 22,121 galaxies from the Third Reference Catalog of Bright Galaxies (RC3, de Vaucouleurs et al. 1991), including Hubble types, but are investigating ensemble properties rather than environment, which would require a more restricted sample due in part to the inhomogeneity of the RC3).

Throughout, the standard spatial geometry is assumed, with Euclidean space,  $\Omega_{\rm matter}=0.3,~\Omega_{\Lambda}=0.7$  and dimensionless Hubble constant h=1, where  $h=H_0/100~{\rm km~s^{-1}~Mpc^{-1}}$ .

## 2 DATA

The SDSS is a project to map  $\pi$  steradians of the northern galactic cap in five bands (u, g, r, i and z) from 3,500–8,900 Å. This will provide photometry for of order  $5 \times 10^7$  galaxies. A multifibre spectrograph will provide redshifts and spectra for approximately  $10^6$  of these. A technical summary of the survey is given in York et al. (2000). The telescope is described in Gunn et al. (2006). The imaging camera is described in Gunn et al. (1998). The photometric system and calibration are described in Fukugita et al. (1996), Hogg et al. (2001), Smith et al. (2002), Ivezić et al. (2004) and Tucker et al. (2006). The astrometric calibration is in Pier et al. (2003) and the data pipelines are in Lupton et al. (2001), Lupton (2007) for the deblender, Frieman et al. and Schlegel et al. (in preparation).

The targeting pipeline (Strauss et al. 2002) chooses targets for spectroscopy from the imaging. A tiling algorithm (Blanton et al. 2003) then assigns the spectroscopic fibres to the targets, the main source of incompleteness being the minimum distance of 55 arcsec between the fibres. This causes about 6% of galaxies to be missed; those that are will be biased towards regions with a high surface density of galaxies. The algorithm gives a more uniform completeness on the sky than a uniform tiling by taking into account large scale structure, but the effect is still present. The other main source of incompleteness is galaxies blended with saturated stars, which is

a 1% level effect. The overall spectroscopic completeness is therefore estimated to be over 90% (Strauss et al. 2002).

The SDSS galaxies with spectra consist of a flux-limited sample, Main, with a median redshift of 0.104 (Strauss et al. 2002); a Luminous Red Galaxy sample (LRG), approximately volumelimited to  $z\approx 0.4$  (Eisenstein et al. 2001); and a quasar sample (Richards et al. 2002). The limiting magnitude for the Main spectra is r<17.77, which is substantially brighter than that for the imaging so the redshift completeness is almost 100%. A typical signal-to-noise value is >4 per pixel and the spectral resolution is 1800. The redshifts have an RMS accuracy of  $\pm 30~{\rm km~s}^{-1}$ .

We use galaxies from the Main Galaxy Sample. The data are extracted from the New York Value-Added Galaxy Catalogue (VAGC, Blanton et al. 2005a). They are masked, extinction- and K-corrected in the same way as the datasets in Ball et al. (2006, hereafter B06). There is no correction for evolution, but as the redshifts are limited to  $z \lesssim 0.1$  its effects are not large. Similarly, there is no correction for dust, but this is mitigated by the requirement that the galaxy axis ratio be less than that of an E7 galaxy, as described in B06.

#### 2.1 Galaxy Environment

The masking of the dataset as in B06 leaves a sample of 489,123 galaxies. These are matched to the galaxies in the Pittsburgh-CMU Value Added Catalogue (VAC, http://nvogre.phyast.pitt.edu/dr4\_value\_added). The matches were carried out using the unique identification, both in object and date of observation, provided by the spectroscopic plate, mjd and fibre values for each object. The matches were made in order to utilise their measures of the distance from each galaxy to the nearest survey edge, which use a sophisticated algorithm taking into account the full survey mask. Galaxies measured by the VAC as being nearer to a survey edge than their Nth nearest neighbour are excluded to prevent the densities being biased downward near the survey edge or at the higher redshifts in the sample.

We do, however, calculate our own environmental densities, as the VAC density sample is restricted to the range 0.053 < z < 0.093 to gain an improved measure of the star formation rate, which is not considered here. We follow the method of B04: the density is given by  $\Sigma_N = N/\pi d_N^2$ , where  $d_N$  is the distance to the Nth nearest neighbour within  $\pm 1000~{\rm km~s^{-1}}$  in redshift. This is used to minimize contamination from interlopers. Here the value of N used is 5, following B04 who choose this value to approximate Dressler (1980) who uses N=10 before correction for superimposed galaxies. We bin the sample in steps of 0.5 over the range  $-1.5 < \log \Sigma_5 < 1.5$ , a factor of 1,000 in density.

We set a limiting absolute magnitude for galaxies to be counted as neighbours of  $M_r-5\log h<-19.5$ , corresponding to one magnitude fainter than the value of  $M^*$  found for the overall Schechter fit to the galaxy luminosity function of B06. The corresponding limiting redshift, at which a galaxy of this magnitude has an apparent magnitude r=17.77 is z<0.0889. This gives a sample volume-limited to a distance comparable to the z<0.08 of B04. We also require z>0.001 to exclude very local objects. We measure densities for galaxies in the range  $M_{-2}^{*+3}$ , i.e.  $-22.5 < M_r - 5\log h < -17.5$ , binning in steps of one magnitude. This again is similar to the range of  $-22.23 < M_r - 5\log h < -17.23$  of B04.

## 2.2 Galaxy Colour and Morphology

We use u-r colour following B04 and Baldry et al. (2004b), who find that the galaxy population is well described as the sum of two Gaussians in u-r, with an optimal colour separator of 2.22 (Strateva et al. 2001). We use the model colours from the same dataset as B06, extinction- and K-corrected, as in that paper, to a rest-frame band-shift of z=0.1, denoted throughout in the plots by  $(u-r)_{0.1}$ , and in the text by u-r. The model colours are derived from the SDSS model magnitudes. For each galaxy these are derived from the best fitting of a de Vaucouleurs (de Vaucouleurs 1948) or exponential profile (Freeman 1970).

For morphology, we use three measures: the inverse concentration index,  $CI_{inv}$ , the Sérsic index, n and the Hubble type. The  $CI_{inv}$  and Sérsic index provide a measure of morphology that, while simple, is available for the full r < 17.77 sample.  $CI_{inv}$  is directly from the SDSS DR4 and is given by  $R_{50}/R_{90}$  where  $R_N$ is the N% light Petrosian radius (see, e.g. Stoughton et al. 2002). The inverse is used because it has the range 0-1. The Sérsic index, from the VAGC, is the exponent in the formula for a generalised galaxy light profile given by Sérsic (1968), or more recently in e.g. Graham & Driver (2005). Because n is an exponent, and the bimodality shows more clearly when it is done so, n is binned logarithmically, as with the density. As with the colours, these are binned appropriately, giving bins of  $0.23 < CI_{\rm inv} < 0.58$  in steps of 0.07 and  $-0.25 < \log n < 0.75$  in steps of 0.2. We truncate the Sérsic index at  $\log n = 0.75$  to avoid a spike in the number of galaxies in the VAGC data with  $\log n \sim 0.77$ . Their data is also truncated at n = 6 (log n = 0.778). Parameters other than colours are measured in the r band, since this band is used to define the aperture through which Petrosian flux is measured for all five bands.

The ANN morphologies used were also the same as those in B06, assigned as in Ball et al. (2004) and updated as described in B06. The types assigned correspond to the Hubble types E=0, S0=1, Sa=2, Sb=3, Sc=4, Sd=5 and Im=6. As described in B06, there is bias away from the ends of the scale, particularly for late types. This is probably due to the dominant contribution of the concentration index in the training set, which shows a similar bias, and the relative lack of types of Sd or later in the training set, about 5% of the total (Fukugita et al. 2007) in part due to the r band selection of the SDSS instead of the more commonly used bluer bands. Hence the latest types assigned have  $T_{\rm ANN} \sim 4.5$ . Fig. 1 shows a random sample of five galaxies from each T type, rounded to the integers 0–4. We bin the ANN morphologies in five bins from -0.5– 4.5. The colours are also binned in five bins. Unlike the other measures presented, the limiting magnitude for the ANN morphologies is r < 15.9, as this was the faintest level to which the visually assigned training set was generated. Of the galaxies studied here, 13,655 have a value for  $T_{\rm ANN}$  and a valid density. Combined with the absolute magnitude limit of  $M_r - 5\log h < -17.5$ , these limits ensure that there is no extrapolation from the ANN training set in apparent or absolute magnitude.

For each set of measurements, the galaxies are required to have values within the ranges of the bins of all quantities that are binned, i.e. density, luminosity, and one or both of colour and morphology. This ensures that each related figure is showing the same galaxies. The resulting samples consist of 79,553 galaxies for u-r, 79,606 for  $CI_{\rm inv}$ , 75,861 for Sérsic index and 13,655 for  $T_{\rm ANN}$ . For the residuals in u-r and morphology, requiring both colour and morphology to be within the bin ranges reduces the sample sizes to 79,495, 75,753 and 13,638 respectively.

## 4 N. M. Ball et al.

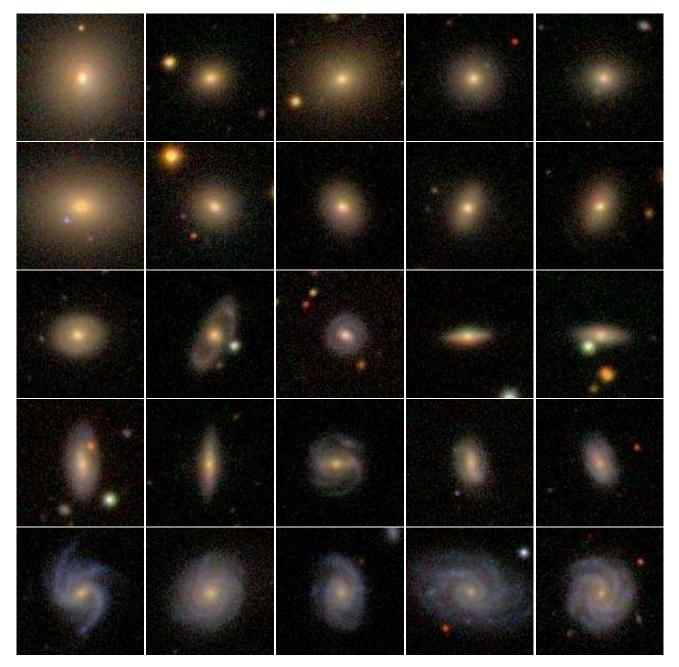


**Figure 1.** SDSS cutout images showing five random galaxies of each of the T-types 0–4 (rounded to the nearest integer) on respective rows. The T types correspond to Hubble types E, S0, Sa, Sb and Sc. This shows the typical quality of the data used in determining the SDSS object parameters used in training the artificial neural network to assign the types. A larger selection of similar images can be found in Fukugita et al. (2007).

## 2.3 Data Fitting

The data points for the histograms of colour and morphology for bins of  $\log \Sigma_5$  and  $M_r$  are fitted with a double Gaussian using a simplex search algorithm over the ranges  $0.5 < u-r < 4.0, 0.23 < CI_{\rm inv} < 0.58, -0.25 < n < 0.75$  and  $0 < T_{\rm ANN} < 4.5$ . The number of galaxies outside these ranges is small, being less than 1% of the total. The fits involve six parameters and are given by

$$A N(\overline{x}_1, \sigma_1) + B N(\overline{x}_2, \sigma_2),$$
 (1)

where the  $N(\overline{x},\sigma)$  are Gaussians with mean  $\overline{x}$  and standard deviation  $\sigma$  and A and B are scalars. Whereas B04 constrain the  $\sigma$  values

of the Gaussians to be functions of  $M_r$  only, here we do not apply any restrictions on the parameters of the two Gaussians in one plot relative to any others. The fits do not utilise the extreme ends of the distributions, where the number of galaxies is negligible.

Again following B04, the  $1\sigma$  error bars for each bin are given by  $\sqrt{N_{\rm bin}+2}$  where  $N_{\rm bin}$  is the number of galaxies in that bin. This is an approximation of the Poisson error for small number statistics.

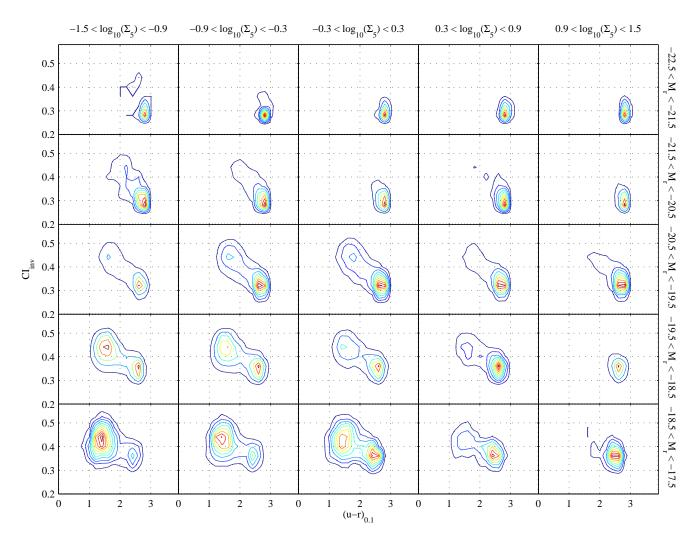


Figure 2. Contour plot of Petrosian inverse concentration index,  $CI_{\text{inv}}$ , versus rest-frame u-r colour, subdivided into panels by environmental density,  $\Sigma_5$  and absolute magnitude,  $M_r$ . The sample consists of 79,606 galaxies. The contours are normalised to the numbers of galaxies in each panel, so small numbers lie outside the lowest contour.

## 3 RESULTS

## 3.1 Two-Dimensional Distributions

Figs. 2–4 show colour versus morphology ( $CI_{\rm inv}$ , Sérsic n and  $T_{\rm ANN}$  respectively) for the sample, divided into panels according to density and luminosity. It is clear that there is a broad division into two populations. This division justifies the treatment below of the galaxies as two populations modelled by a double Gaussian, which is used in  $\S 3.2 – \S 3.4$  below to quantify the trends seen in more detail.

In Fig. 2, the populations are approximately centred on  $u-r\sim 2.75,\,CI_{\rm inv}\sim 0.35$  and  $u-r\sim 1.5,\,CI_{\rm inv}\sim 0.45$ . These correspond to the red, early-type and blue, late-types. As expected, there are few red galaxies with high  $CI_{\rm inv}$  or blue galaxies with low  $CI_{\rm inv}$ , and there is little dependence of each population centre on luminosity or density. What does change radically is the relative numbers of galaxies in each population, which is emphasized here by the normalisation applied to the contours in each panel. Blue colours and diffuse morphologies dominate in galaxies of low luminosity in low density environments. They are almost entirely absent in luminous galaxies and in high-density regions.

Fig. 3 shows a similar pattern, although the sense of n is inverted compared to  $CI_{\rm inv}$ . The truncation in the Sérsic index at  $\log n < 0.75$  (§2.2) is visible, although the contours show that few galaxies are excluded. At fainter magnitudes,  $M_r \gtrsim -19.5$ , the visual overlap between the populations is lower in n than in  $CI_{\rm inv}$ .

Fig. 4 shows that there are again similar patterns in  $T_{\rm ANN}$  morphology. Types  $0 \lesssim T_{\rm ANN} \lesssim 2$ , i.e., E–Sa, are all approximately the same colour, although the incidence of types  $T_{\rm ANN} \gtrsim 1$  decreases at bright magnitudes  $M_r \lesssim -20.5$ . There are relatively few galaxies at the faint end,  $-17.5 < M_r < -18.5$  due to the brighter r < 15.9 magnitude limit for  $T_{\rm ANN}$  compared to r < 17.77 for  $CI_{\rm inv}$  and n.

#### 3.2 Gaussian Fits

Fig. 5 shows the rest-frame u-r colour distribution, subdivided by density  $\log \Sigma_5$  and luminosity  $M_r$ . The distributions are clearly bimodal and well fit by a sum of two Gaussians, confirming the idea of two separate populations described by numerous authors (e.g. Baldry et al. 2004b). As expected, the fraction of blue galaxies decreases with density. The position of the blue peak moves redwards

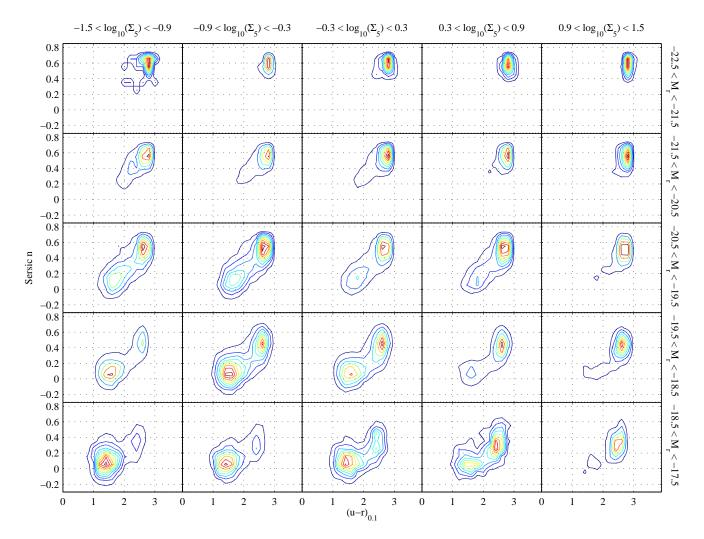


Figure 3. As Figure 2, but with  $CI_{inv}$  replaced by the logarithmic Sérsic index,  $\log n$ , for 75,861 galaxies. The truncation of the data at  $\log n = 0.75$  (§2.2) is visible.

from  $u-r\approx 1.5$  to  $u-r\approx 2.25$  and that of the red peak stays approximately constant, with just a slight reddening from  $u-r\approx 2.5$  to  $u-r\approx 2.75$ . Unlike the peaks, the position of the minimum between the two distributions stays constant, although in the higher density and luminosity bins the exact position of the minimum is unclear. Versus luminosity, a similar trend is seen with the red peak moving slightly bluewards and dropping in fraction with decreasing luminosity and the blue peak becoming bluer. Bright galaxies at  $M_r-5\log h<-21.5$  are relatively rare as are faint galaxies due to the r<17.77 limit for spectra.

The figure represents an update of fig. 1 of B04, using DR4 rather than DR1 and with the differences described in §2 above. As mentioned, B04 find that at fixed luminosity the mean colours of the two distributions are nearly independent of density, with just a weak trend for colours to become redder at high densities, but that the fraction of red galaxies rises sharply at all luminosities. As expected, our plot shows the same trends.

Figs. 6–8 show the same as Fig. 5 but for the  $CI_{\rm inv}$ , Sérsic n and  $T_{\rm ANN}$  morphologies respectively, i.e., they show the morphology-density relation subdivided by luminosity.

As with colour, the concentration index shows clearly bimodal distribution, although significant overlap between the populations

causes a unimodal appearance in some of the panels. The plots show peaks at  $CI_{\rm inv} \sim 0.3$  and  $CI_{\rm inv} \sim 0.43$ , corresponding to the de Vaucouleurs elliptical galaxy profile and the exponential spiral disc profiles, respectively. As expected, early-type galaxies dominate at high density and high luminosity.

The Sérsic index shows a bimodal distribution at all densities and all but the highest and lowest luminosities. The indices n=4 (log n=0.60) and n=1 (log n=0) correspond to the de Vaucouleurs and exponential profiles. The peaks in the distribution are close to these values, but slightly nearer the overall mean, in a similar manner to  $CI_{\rm inv}$ .

For  $T_{\rm ANN}$ , a sum of two Gaussians is now a worse fit to the data, with a clear excess of galaxies at  $T_{\rm ANN} \sim 1$  at densities  $\log \Sigma_5 \gtrsim -0.3$ . The expected dominance of early types at high density is seen and the peak narrows with density. The late-type peaks becomes lower and earlier, in a similar manner to the reddening of the blue peak in u-r. The lack of (or less clear) division into a bimodal population suggests that if galaxies really are divided into just two dominant populations then either (1) the  $T_{\rm ANN}$  is insensitive to it, spreading between the two; (2) that  $T_{\rm ANN}$  is more sensitive to transitional states between the two, such as S0 galaxies, than colour, or (3) the  $T_{\rm ANN}$  is an intrinsically 'fuzzy'

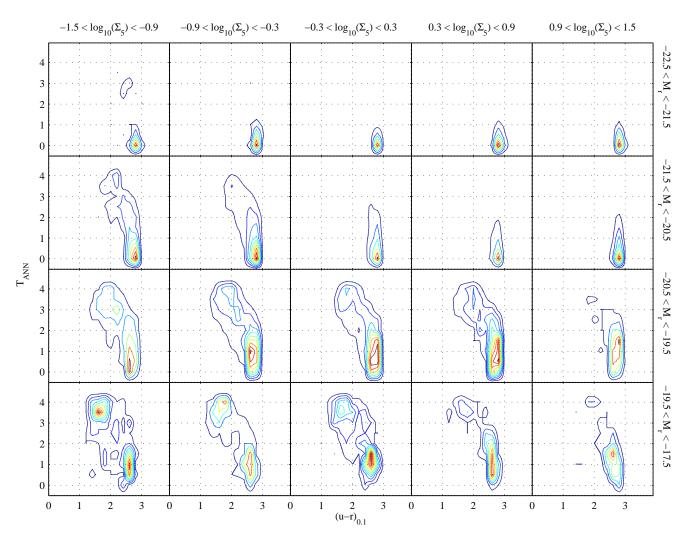


Figure 4. As Figure 2, but with  $CI_{\text{inv}}$  replaced by the Hubble T type assigned by an artificial neural network,  $T_{\text{ANN}}$ , and the faintest two bins combined due to the low number of galaxies in the faintest bin. The sample size is 13,655 galaxies.

measure, resulting in a inevitable spread across types. If (2) is correct, such a transitional state must then be rare and/or brief in colour space for the clear division in colour to be seen as S0 galaxies are not rare. That the transitional population is clearest at higher densities is also consistent with it being S0s. (3) is less likely for the overall population, i.e. one can split E/S0 from spiral, but the excess over Gaussian at  $T_{\rm ANN} \sim 1$  and at very late types supports the 'fuzzy' nature of the Hubble type classification. The spread is not likely to be an artefact of typing via neural network, as these were shown (e.g. Storrie-Lombardi et al. 1992; Naim et al. 1995; Ball et al. 2004) to perform with an RMS spread between true type and assigned type no different to that between human classifiers.

In most of the plots in Figs. 5–8, the reduced  $\chi^2$  values, expected to be around 1 or less, of the double Gaussian fit are large. This was also seen in the  $\chi^2$  for fitting the bivariate LF in B06. As with those results, this is probably due to the small size of the error bars resulting from the large number of galaxies in the sample, indicating that the fitting function used is only an approximation to the data. What is clear is that the data is better fitted by two Gaussians than, say, one.

#### 3.3 Red Fraction, Mean, Dispersion

Figs. 9–11 show some of the trends in Figs. 5–8 more clearly. The  $\pm 1\sigma$  error bars are calculated by finding the point at which the  $\chi^2$  for the fit increases by 1 around the minimum for each parameter in turn. The shape of the  $\chi^2$  is assumed to be parabolic, which is a good approximation, although it assumes that the  $\chi^2$  is minimized for the other parameters whilst the one under study is being varied. However, these approximations will tend to overestimate the errors, so it is good as a conservative estimate.

The top left panel of Fig. 9 shows the fraction of red galaxies for  $M_r$  versus  $\Sigma_5$  for u-r. The fraction is given by the ratio of the areas under the two Gaussians, which is given by A/(A+B) assuming that approximately the whole area under each Gaussian is populated by galaxies (the normalised areas are 1). This is seen to be true in Figs. 5–8. The fraction rises with density, as expected, and rises in a similar way over all luminosities, although the brightest galaxies at  $-22.5 < M_r - 5\log h < -21.5$  are slightly noisy. The trends are similar to those in the left hand panel of fig. 2 in B04.

The top left two panels of Fig. 10 show the mean u-r colours  $\overline{x}_1$  and  $\overline{x}_2$  in a similar way for the two Gaussians. The mean colour

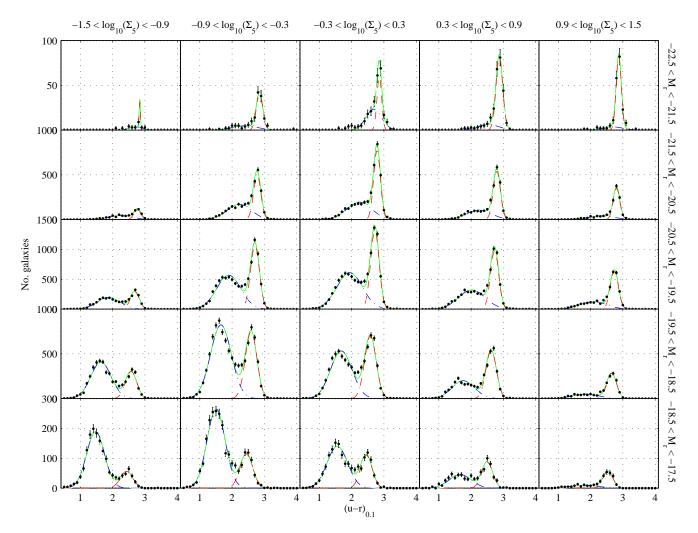


Figure 5. Numbers of galaxies for u-r subdivided by  $\Sigma_5$  and  $M_r$ . The points are the number of galaxies in each bin; the error bars are given by  $\sqrt{N_{\rm bin}+2}$  where  $N_{\rm bin}$  is the number of galaxies in that bin; the solid line is the best fit of the sum of two Gaussians; the dot-dash and dashed lines are the individual Gaussians. The vertical axes within each row of panels are given equal heights for clarity. This plot is similar to that of Balogh et al. (2004), but for DR4 as opposed to DR1. The trends seen are very similar, as expected, because DR4 is a superset of DR1.

for the red galaxies is approximately independent of density (as seen in Fig. 5), with just a slight trend for redder colours at higher densities. The blue galaxies show a more distinct reddening towards the highest densities. This is similar to fig. 3 of B04.

The top left hand two panels of Fig. 11 show the u-r dispersions  $\sigma_1$  and  $\sigma_2$ . For red galaxies the dispersions are low and for lower luminosities decline at the highest density, whilst those for the blue galaxies are higher, slightly increasing at the highest density for low luminosity. The dispersions for red galaxies also show a clear decrease with increasing luminosity.

The remaining panels of Figs. 9–11 show the same as u-r but for the  $CI_{\rm inv}$ , Sérsic n and  $T_{\rm ANN}$  morphologies. Each measure of morphology shows a similar behaviour. In Fig. 9, the early-type fraction shows some increase with density in a similar way to the red fraction, whereas the late-type fractions (not shown) are noisy.

In Fig. 10 the mean type for the early-type galaxies is seen to be approximately independent of density at fixed luminosity in the same way that colour was for the red galaxies. This hints that the same population is being seen, which is consistent with a distinct bright, concentrated, early spectral type, red population. The

late types change little with density, the  $CI_{\rm inv}$  and  $T_{\rm ANN}$  becoming earlier but the Sérsic n showing no trend. The similarity of the patterns seen suggests that in terms of the effect of environmental density, colour is closely correlated with morphology, but that there could be a residual relation.

Fig. 11 shows that for morphology the dispersions do not show any obvious trends with density. For u-r, this justifies the constraint in B04 for the the dispersion not to vary. (B04 also find little change if they relax this constraint.) Some of the larger changes are due to the widths of individual Gaussians being poorly constrained by either significant overlap between them or by low numbers of galaxies.

## 3.4 Residual Colour- and Morphology-Density

The residual relations are calculated by binning the galaxies into a 2-dimensional grid of colour and morphology, using the same histogram bins as in Figs. 5–8. The mean density  $\mu_{ij}$  in each bin is calculated, along with the marginal averages as a function of colour bin  $(\mu_i^c)$  and of morphology bin  $(\mu_j^m)$ , using the densities for the in-

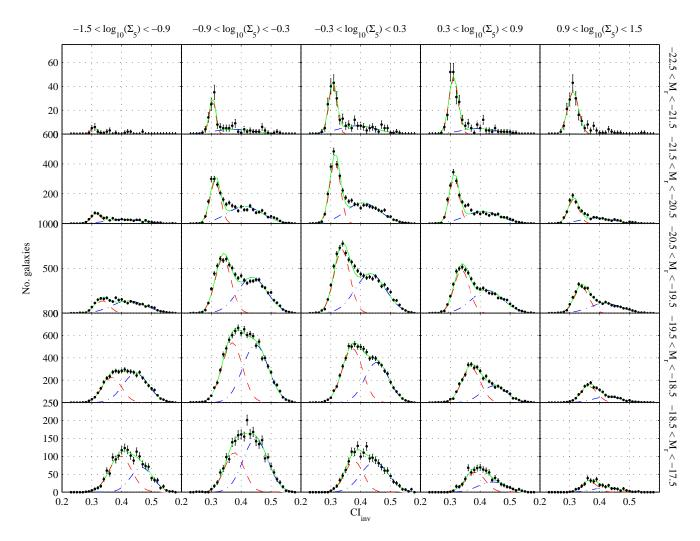


**Figure 6.** As Fig. 5 but for  $CI_{\mathrm{inv}}$ .

dividual galaxies in each so that the bins are correctly weighted. In order to factor out the colour-dependence of density, one divides each mean density  $\mu_{ij}$  by the appropriate marginal average  $\mu_i^c$ . A re-calculation of the marginal dependence of density on colour would then give all ones, whereas a re-calculation of the marginal dependence on morphology will yield the residual morphology-dependence of density after that due to colour has been removed. By instead dividing out the morphology-dependence in an equivalent way, the residual colour dependence may be calculated. The errors on each point are the  $1\sigma$  dispersion of the values of the bins which are averaged to give that point.

Fig. 12 shows the residual relation for u-r on removal of morphology. There is a definite trend in density with colour, consistent with numerous earlier studies (e.g. Kauffmann et al. 2004; Blanton et al. 2005b) in which the colour was a strong predictor of environmental density. As expected, the density increases for redder galaxies. The error bars are still relatively large, reflecting the less certain nature of  $\Sigma_5$  compared to colour.

Fig. 13 shows the morphology-density relation after the removal of the change in density due to the change in colour with morphology. In contrast to colour, the residual relation is consistent with a value of one, i.e. no residual relation. This means that

there is no evidence for a change in morphology that is not correlated with a change in colour.

## 3.5 Comparison to Previous Work

Besides B04, who presented the colour-density relation for the EDR and for whose results ours broadly represent an update to the SDSS DR4 (§3.3 and §3.4 above), substantial work involving similar measures of colour and morphology with comparison to density has been carried out by Goto et al. (2003) and Park et al. (2007).

Goto et al. (2003) present the morphology-density relation for the SDSS EDR. They assign morphology using the inverse concentration index, as used here, and a preliminary version of the texture parameter described by Yamauchi et al. (2005). The latter is corrected for elliptical isophotes and gives an improved correlation to visual morphology. The galaxies are divided into early, intermediate, early disc and late disc. The sample is volume-limited to  $M_r - 5\log h < -19.9$  in the redshift range 0.05 < z < 1 and contains 7,938 galaxies. This compares to our values of  $M_r - 5\log h < -19.5$ , 0.001 < z < 0.0889 and 13,655 galaxies. The same  $\Omega_{\rm matter} = 0.3$ ,  $\Omega_{\Lambda} = 0.7$  Euclidean cosmology is used. Their density estimator is three dimensional.

They find the expected trend of increasing early-type fraction

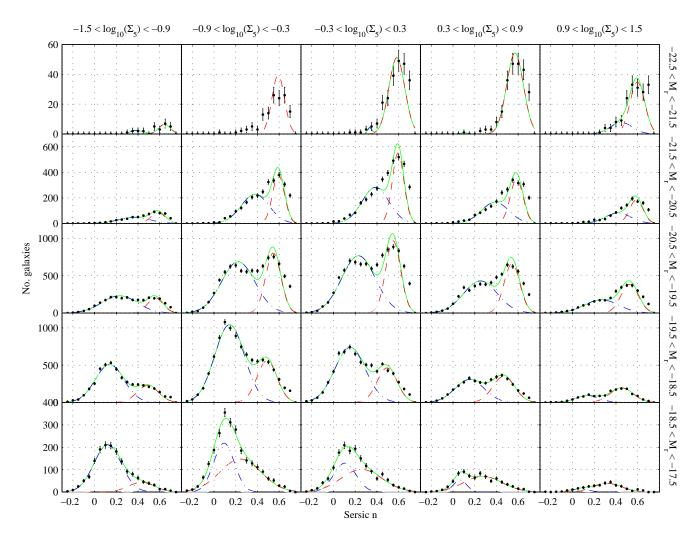


**Figure 7.** As Fig. 5 but for Sérsic n.

with increasing density, and also two characteristic scales, giving three density regimes. In the lowest density regime, the relation is less noticeable. In the intermediate density regime, intermediate type galaxies increase with density and spirals decrease. In the densest regime, the intermediate types decrease and the early types increase. Thus the morphology is little affected in the low density regime, then subject to a mechanism which inhibits star formation and turns spirals into intermediate types in the intermediate density regime, then a third process decreases these types and increases early types in the dense regime. Our work is consistent with this, with the bridge between the two bimodal populations resembling the intermediate types described here. It is difficult to compare quantitatively, however, as the density measures are different.

Park et al. (2007) study numerous galaxy properties as a function of environment in various volume-limited samples containing up to 80,479 galaxies for 0.025 < z < 0.11 using a subset of the SDSS DR5. The galaxy properties studied include the  $(u-r)_{0.1}$  colour and morphology assigned using the colour gradient method of Park & Choi (2005). Their measure of density is obtained using an adaptive smoothing kernel, so again an exact quantitative comparison with our results would be difficult. Their fig. 9 shows the fraction of early-type galaxies (as defined in Park & Choi (2005)) as a function of density and luminosity. The result shows the same

trends as our Fig. 5, with a monotonic increase in early-type fraction with density and luminosity, and the trend lines separated by luminosity approximately parallel to each other. However, they also fix both luminosity and morphology and then find little residual dependence of properties on environment, except for a sharp decrease in late types at the bright end.

#### 4 DISCUSSION

Considering the number of galaxies, the variety of their properties and environments and the quality of the SDSS data, the rest-frame colour histograms are well fit by a simple sum of two Gaussians. This result is also seen by B04 and others and strongly suggests two underlying populations of galaxies. This is consistent with the patterns seen in the LFs in B06 (their figs. 2, 3, 4 and 6 show the LF bivariate with  $T_{\rm ANN}$ ,  $CI_{\rm inv}$ , Sérsic n and  $(u-r)_{0.1}$  respectively). There, an early morphological type, concentrated, early spectral type, red, high Sérsic index population of galaxies is evident and the LFs binned in absolute magnitude and plotted against their second parameter often show bimodality.

One of the main questions asked in this paper is whether the morphology reveals anything that the colours do not. Compared to

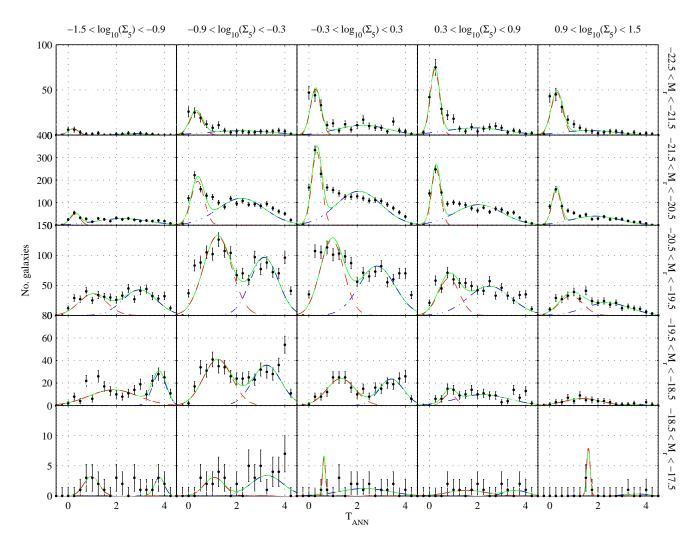


**Figure 8.** As Fig. 5 but for  $T_{\mathrm{ANN}}$ .

u-r, the  $CI_{\mathrm{inv}}$  and Sérsic n also show clearly bimodal distributions, although the  $CI_{\mathrm{inv}}$  plot becomes unimodal at fainter magnitudes and low densities. There are no obvious residual relations when those due to colour are removed, thus these measures of morphology appear not to be predictive of environment beyond their correlation to colour.

When the  $T_{\rm ANN}$  morphology-density relation is plotted the distributions are less bimodal, ranging from looking similar to the plots for colour to being not bimodal at all. There are various possible reasons for this, including (1) the morphology may be less sensitive to the processes producing the bimodal population in colour, being intrinsically spread when compared to the colour-producing physics; (2) there may be more than two populations, the third or higher to which colour may not be sensitive (an example might be S0 galaxies, which are almost as red as ellipticals); or (3) the neural network morphological types might be spread or biased versus the true types. The last point is not thought to be likely (Ball et al. 2004). It is difficult to distinguish between the intrinsic spread or more populations possibilities, although the fact that some of the bins are more bimodal than others favours the third population idea. Here neither possibility is ruled out and indeed both could be occurring. More detailed investigation of the morphology-colour-density relationship may be useful, but it may remain the case that the morphologies are simply intrinsically too 'fuzzy' to show the underlying populations as clearly as the colour. That said,  $T_{\rm ANN}$  has larger error bars, so the formal goodness of fit is not necessarily worse than that for u-r,  $CI_{\rm inv}$  and n.

This spreading of Hubble types between the two populations is also seen by various other workers. In the Millennium Galaxy Catalogue (MGC, Liske et al. 2003), Driver et al. (2006) study a sample of 3314 galaxies with eyeball Hubble types at B<19 and find that, while types E/S0 (bulges) exclusively occupy the early-type peak and Sd and later (discs) the late-type peak, the Sa–Sc, which are a mixture of bulge and disc, are spread between the two peaks. Also in the MGC, Ellis et al. (2005) study a well-defined sample of 350 galaxies and find, using multivariate statistical analysis of the galaxy properties, that only two populations, corresponding to early and late types, are justified, and the late types (Sa–Irr) are smoothly spread within the late-type region of parameter space. In a sample of 1,246 galaxies with Hubble types from the Revised Shapely-Ames catalogue, van den Bergh (2007) similarly find a continuum of Hubble types but a bimodality in colour.

In a sample of 22,121 galaxies from the Third Reference Catalogue of Bright Galaxies, Conselice (2006) finds that the best three parameters with which to classify galaxies are mass, star formation and merger history. The Hubble type correlates most strongly with

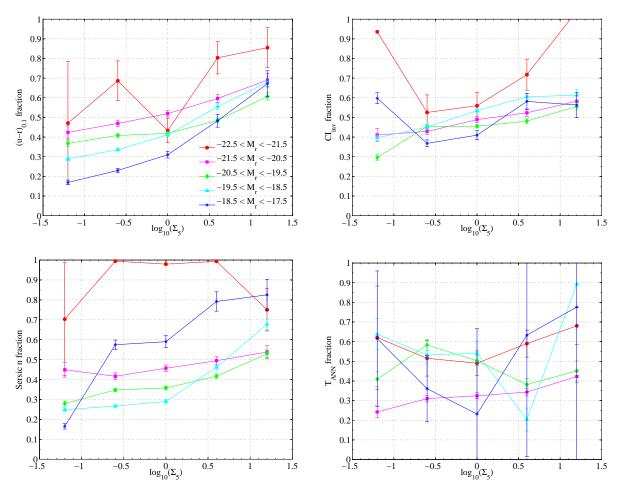


Figure 9. Red and early-type galaxy fractions in each  $M_r$  bin versus  $\Sigma_5$  for u-r,  $CI_{\rm inv}$ , Sérsic n and  $T_{\rm ANN}$ . The error bars are  $1\sigma$ . The left hand panel shows a similar upward trend to fig. 2 of B04.

stellar mass,  $(U-B)_0$  and  $(B-V)_0$  colour. They also (his fig. 10) confirm the intrinsic spread in morphology when compared to other properties such as colour, showing that morphology is at least to some extent independent of the other parameters.

Baldry et al. (2004a) discuss the work in Baldry et al. (2004b) and B04 and agree with the interpretation of morphology, in the sense that 'whatever processes give rise to the blue/red distribution should also give rise to *distributions* in morphology', although they go on to say that 'thus, S0 or Sa galaxies could have a probability of belonging to one or the other distributions and should not be considered as classes'.

The physics giving the bimodal population in colour is thought to be that red galaxies have a passively evolving old stellar population and are formed by major mergers. The blue galaxies are undergoing star formation and less violent accretion events. Galaxies can change from blue to red and when they do they do so rapidly, leaving few galaxies in between the two populations. B04 go on to propose that 'most star forming galaxies today evolve at a rate that is determined primarily by their intrinsic properties, and independent of environment', which is consistent with the results here. The morphology may be seeing extra physics at work, for example rampressure stripping of gas from a galaxy infalling into a cluster can turn a spiral into an S0 rather than an elliptical, even though they are almost as red. S0s are sufficiently common that they should show

up as a component in the plots in this paper if they indeed form a component distinct from other galaxies. In comparison to simulations, only recently have semi-analytic models begun to produce bimodal populations matching those observed (e.g. Cattaneo et al. 2006), so there may still be much to be gained by a detailed intercomparison between the two.

The ANN types are biased away from very early or late types, but not to an extent large enough to affect the overall trends seen here. This is thought to be due to the importance of the concentration index in the training set, which has a similar bias. A larger training set for morphology is needed, particularly for very late types of type Scd or later, corresponding to  $T_{\rm ANN} \geqslant 4.5$ . Our training set was based on the SDSS EDR version of the catalogue of Fukugita et al. (2007). However, their published version, while based on DR3 and 40% larger at 2658 galaxies instead of 1875, would be unlikely to significantly improve our results due to the intrinsic spread in  $T_{\rm ANN}$  and the r-band object selection of the SDSS, which limits the Scd or later types to 5.2% of the sample. They compare this to 10.6% from the earlier B-band study of Fukugita et al. (1998).

Here the model u-r colour was used. Driver et al. (2006) showed that the core u-r, measured using the PSF colour, provides a cleaner separation for their sample when used in conjunction with the Sérsic index. The same may be true here if that u-r

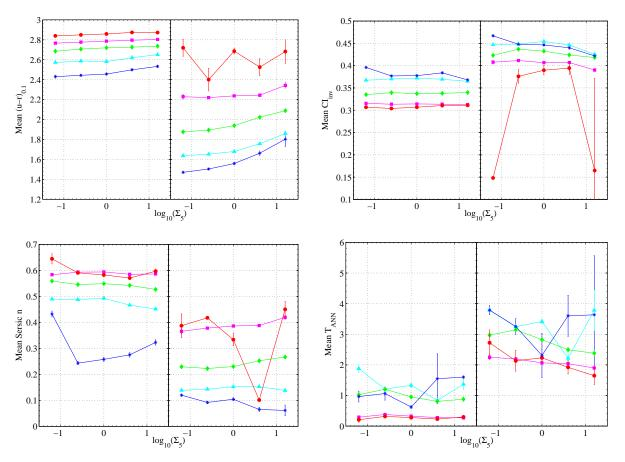


Figure 10. Mean colour and type in each  $M_r$  bin versus  $\Sigma_5$  for u-r,  $CI_{\mathrm{inv}}$ , Sérsic n and  $T_{\mathrm{ANN}}$ . The left hand sides of each panel show red/early-type galaxies and the right hand sides show blue/late-type. The error bars are  $1\sigma$ . The left hand sides of the u-r panel is similar to fig. 3 of B04. The magnitude bins are the same as for Fig. 9.

were used, although the model u-r is cleaner than the Petrosian u-r, for which we also generated results. Driver et al. (2006) also argue that the two fundamental components are, rather than red and blue galaxies, bulges and discs. This is consistent with the results here. However, it is not necessarily that simple, as Drory & Fisher (2007) differentiate classical and pseudobulges, which have different formation mechanisms, and find that, for types Sa-Sbc for a given bulge-to-total light ratio, the former are predominantly in red galaxies and the latter in blue, i.e., the bimodal distribution is not simply due to the bulge to disk ratio.

## 5 CONCLUSIONS

Galaxy properties are studied as a function of environment in the SDSS, specifically the relations between u-r restframe colour, morphological type and the environmental density. The colour is given by the restframe value of u-r. The morphology is in the form of the inverse concentration index,  $CI_{\rm inv}$ , the Sérsic index, n and the Hubble T type,  $T_{\rm ANN}$ , the latter assigned by a trained artificial neural network. The density is the  $\Sigma_5$  surface density of galaxies measured by the fifth nearest neighbour brighter than an r band absolute magnitude of  $M_r - 5\log h = -19.5$ . The range of density probed covers all environments from the cores of rich clusters to the field. The colour results are similar to those of Balogh et al. (2004) (B04) but here these are extended to galaxy morphology.

Subdivision of the population by density and luminosity shows a clear bimodal distribution in the colour-morphology plane. For each subsample we fit the colour and morphology by a sum of two Gaussians. The well-known colour-density and morphology-density relations are seen. The colour is well fit by the Gaussian sum, confirming two underlying populations, one red and one blue, as seen by B04. The mean colour of the red population is approximately constant but the blue population gets slightly redder with increasing density. The relations are seen at high significance over the range of densities probed, thus confirming that they extend into the field and are not just present in galaxy clusters.

Compared to u-r,  $CI_{\mathrm{inv}}$  and n, the  $T_{\mathrm{ANN}}$  morphology is less obviously fit by the sum of two Gaussians, suggesting one or more of the possibilities (1) three or more populations (e.g. early, lenticular and late), (2) sensitivity of the morphology to processes which do not affect the colours, or (3) a higher intrinsic spread in morphology compared to two underlying populations and physical processes.

While the  $CI_{\mathrm{inv}}$  and Sérsic n to some extent separate the two main galaxy populations, certainly more cleanly than the Hubble type, both still suffer from extensive overlap in the populations. Figs. 2–4 show that, rather than using a single colour or morphology, improved separations should be obtained using a division in the plane of colour and morphology rather than any single measure. In its simplest form in Figs. 2–4, this would correspond to the allowance of an oblique line as a separator instead of an axis-parallel

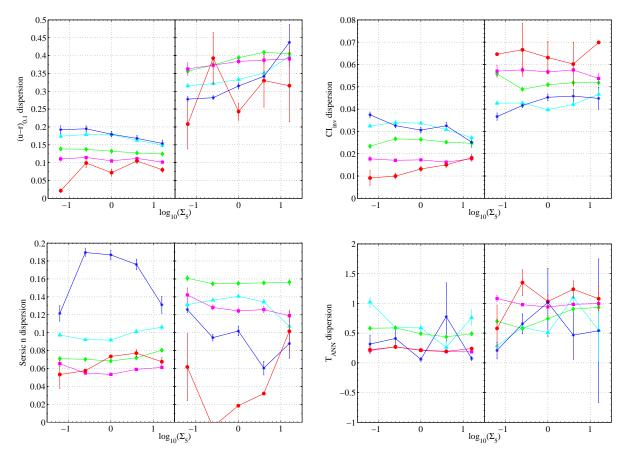


**Figure 11.** As Fig. 10 but for the  $\sigma$  dispersions in the Gaussian fits.

line (c.f. e.g. fig. 6 of Choi et al. (2007), fig. 10 of Baldry et al. (2006), or fig. 15 of Driver et al. (2006), which also show this planar distribution).

The colour-density relation divided into bins by absolute magnitude reproduces the results of B04: the mean colours are independent of density for fixed luminosity but the red fraction increases with increasing density. The fraction of red galaxies increases approximately linearly with density, with parallel slopes of lower fraction for decreasing luminosity. The dispersion in colour for each population is low for red galaxies, increasing with decreasing luminosity and decreasing with density for low luminosity. For blue galaxies it is significantly higher increasing at low luminosity with density. At high luminosity there is now a significant trend with density.

The morphology-density relations divided in this way are similar if the early-type galaxies are red. The early-type galaxy fractions increase in a similar way to the fraction of red galaxies but the trends are noisier. The mean types versus density are similar to colour but the late types do not as obviously get earlier with density, consistent with the colour having a stronger dependence on density than morphology. The dispersions show few significant trends with density.

In u-r there is a clear residual relation of galaxies for both blue and red galaxies with density even after the reddening due to the increase in early types is removed. This suggests that colour has a stronger dependence on density than morphology, in agreement with other studies.

For each of  $CI_{inv}$ , n and  $T_{ANN}$ , there is no evidence of a

residual trend once that due to variation with colour is removed. Therefore, for these data, none of the measures of morphology are predictive of environment beyond their correlation to colour.

## ACKNOWLEDGMENTS

Nick Ball thanks Bob Nichol, Ivan Baldry, and Michael Balogh for useful discussions, and K. Simon Krughoff and Chris Miller for help with the DR4 VAC catalogue. We thank the referee for a comprehensive and constructive report which improved the paper. NMB was funded by a PPARC studentship from 2001–2004 and, with RJB, would like to acknowledge support from NASA through grants NN6066H156 and 05-GALEX05-0036, from Microsoft Research, and from the University of Illinois.

Funding for the SDSS and SDSS-II has been provided by the Alfred P. Sloan Foundation, the Participating Institutions, the National Science Foundation, the U.S. Department of Energy, the National Aeronautics and Space Administration, the Japanese Monbukagakusho, the Max Planck Society, and the Higher Education Funding Council for England. The SDSS Web Site is http://www.sdss.org/.

The SDSS is managed by the Astrophysical Research Consortium for the Participating Institutions. The Participating Institutions are the American Museum of Natural History, Astrophysical Institute Potsdam, University of Basel, Cambridge University, Case Western Reserve University, University of Chicago, Drexel University, Fermilab, the Institute for Advanced Study, the Japan

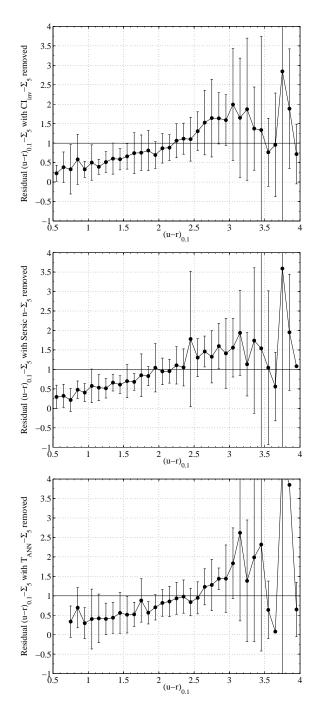


**Figure 12.** Residual density dependence of colour once the dependence due to morphology  $(CI_{\mathrm{inv}}, \mathrm{S\acute{e}rsic}\ n$  and  $T_{\mathrm{ANN}}$  in respective panels) has been removed. The sample sizes are 79,495, 75,753 and 13,638 galaxies respectively. The error bars are the  $1\sigma$  dispersion in the morphology bins, and a value of 1, highlighted by the horizontal line, indicates no residual. There is a clear reddening of colour with density.

Participation Group, Johns Hopkins University, the Joint Institute for Nuclear Astrophysics, the Kavli Institute for Particle Astrophysics and Cosmology, the Korean Scientist Group, the Chinese Academy of Sciences (LAMOST), Los Alamos National Laboratory, the Max-Planck-Institute for Astronomy (MPA), the Max-Planck-Institute for Astrophysics (MPIA), New Mexico State University, Ohio State University, University of Pittsburgh, University

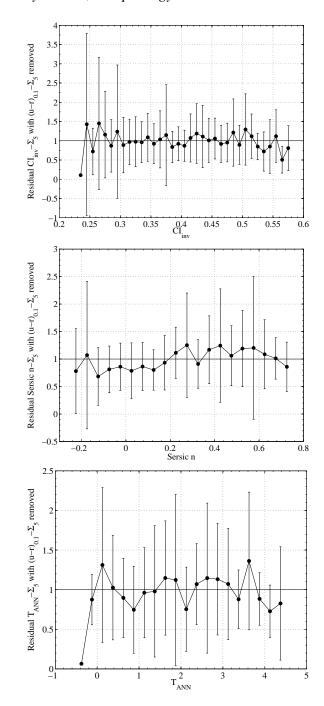


**Figure 13.** As Fig. 12, with the same sample sizes, but for the residual density dependence of morphology once that due to colour has been removed. Unlike colour, here there is no clear trend.

of Portsmouth, Princeton University, the United States Naval Observatory, and the University of Washington.

This research has made use of NASA's Astrophysics Data System.

## REFERENCES

Abbas U., Sheth R. K., 2006, MNRAS, 372, 1749 Adelman-McCarthy J. K., et al., 2006, ApJS, 162, 38 Avila-Reese V., 2007, in Solar, stellar and galactic connections between particle physics and astrophysics Ap&SS Proceedings, Understanding Galaxy Formation and Evolution. Springer, pp 115–165

Baldry I. K., Balogh M. L., Bower R., Glazebrook K., Nichol R. C., 2004a, in Allen R. E., Nanopoulos D. V., Pope C. N., eds, AIP Conf. Proc. 743: The New Cosmology: Conference on Strings and Cosmology Color bimodality: Implications for galaxy evolution. pp 106–119

Baldry I. K., Glazebrook K., Brinkmann J., Ivezić Ž., Lupton R. H., Nichol R. C., Szalay A. S., 2004b, ApJ, 600, 681

Baldry I. K., Balogh M. L., Bower R. G., Glazebrook K., Nichol R. C., Bamford S. P., Budavari T., 2006, MNRAS, 373, 469

Ball N. M., Loveday J., Fukugita M., Nakamura O., Okamura S., Brinkmann J., Brunner R. J., 2004, MNRAS, 348, 1038

Ball N. M., Loveday J., Brunner R. J., Baldry I. K., Brinkmann J., 2006, MNRAS, 373, 845

Balogh M. L., Baldry I. K., Nichol R., Miller C., Bower R., Glazebrook K., 2004, ApJL, 615, L101

Blanton M. R., Berlind A. A., 2007, ApJ, 664, 791

Blanton M. R., Lin H., Lupton R. H., Maley F. M., Young N., Zehavi I., Loveday J., 2003, AJ, 125, 2276

Blanton M. R., et al., 2005a, AJ, 129, 2562

Blanton M. R., Eisenstein D., Hogg D. W., Schlegel D. J., Brinkmann J., 2005b, ApJ, 629, 143

Blanton M. R., Eisenstein D., Hogg D. W., Zehavi I., 2006, ApJ, 645, 977

Boselli A., Gavazzi G., 2006, PASP, 118, 517

Cattaneo A., Dekel A., Devriendt J., Guiderdoni B., Blaizot J., 2006, MNRAS, 370, 1651

Choi Y.-Y., Park C., Vogeley M. S., 2007, ApJ, 658, 884

Christlein D., Zabludoff A. I., 2004, ApJ, 616, 192

Colless M., et al., 2001, MNRAS, 328, 1039

Conselice C. J., 2006, MNRAS, 373, 1389

Cooray A., Sheth R., 2002, PhR, 372, 1

de Vaucouleurs G., 1948, Annales d'Astrophysique, 11, 247

de Vaucouleurs G., de Vaucouleurs A., Corwin H. G., Buta R. J., Paturel G., Fouque P., 1991, Third Reference Catalogue of Bright Galaxies. Volume 1-3, XII, 2069 pp. 7 figs.. Springer-Verlag Berlin Heidelberg New York

Dressler A., 1980, ApJ, 236, 351

Driver S. P., et al., 2006, MNRAS, 368, 414

Drory N., Fisher D. B., 2007, ApJ, 664, 640

Einasto M., et al., 2007, A&A, 464, 815

Eisenstein D. J., et al., 2001, AJ, 122, 2267

Ellis S. C., Driver S. P., Allen P. D., Liske J., Bland-Hawthorn J., De Propris R., 2005, MNRAS, 363, 1257

Erdoğdu P., et al., 2004, MNRAS, 352, 939

Freeman K. C., 1970, ApJ, 160, 811

Fukugita M., Ichikawa T., Gunn J. E., Doi M., Shimasaku K., Schneider D. P., 1996, AJ, 111, 1748

Fukugita M., Hogan C. J., Peebles P. J. E., 1998, ApJ, 503, 518 Fukugita M., et al., 2007, AJ, 134, 579

Goto T., Yamauchi C., Fujita Y., Okamura S., Sekiguchi M., Smail I., Bernardi M., Gomez P. L., 2003, MNRAS, 346, 601

Graham A. W., Driver S. P., 2005, PASA, 22, 118

Gunn J. E., et al., 1998, AJ, 116, 3040

Gunn J. E., et al., 2006, AJ, 131, 2332

Hogg D. W., Finkbeiner D. P., Schlegel D. J., Gunn J. E., 2001, AJ, 122, 2129

Hogg D., 2006, in Le Brun V., Mazure A., Arnouts S., BurgarellaD., eds, The Fabulous Destiny of Galaxies: Bridging Past and

Present What Best Constrains Galaxy Evolution in the Local Universe. p. 41

Ivezić Ž., et al., 2004, Astronomische Nachrichten, 325, 583

Kauffmann G., White S. D. M., Heckman T. M., Ménard B., Brinchmann J., Charlot S., Tremonti C., Brinkmann J., 2004, MNRAS, 353, 713

Lane K. P., Gray M. E., Aragón-Salamanca A., Wolf C., Meisenheimer K., 2007, MNRAS, 378, 716

Liske J., Lemon D. J., Driver S. P., Cross N. J. G., Couch W. J., 2003, MNRAS, 344, 307

Lupton R. H., 2007, AJ, submitted

Lupton R. H., Gunn J. E., Ivezić Z., Knapp G. R., Kent S., Yasuda N., 2001, in ASP Conf. Ser. 238: Astronomical Data Analysis Software and Systems X The SDSS Imaging Pipelines

Martínez H. J., Muriel H., 2006, MNRAS, 370, 1003

Moran S. M., Ellis R. S., Treu T., Smith G. P., Rich R. M., Smail I., 2007, preprint (arXiv/0707.4173)

Naim A., Lahav O., Sodré L., Storrie-Lombardi M. C., 1995, MN-RAS, 275, 567

Oemler A. J., 1974, ApJ, 194, 1

Park C., Choi Y.-Y., 2005, ApJL, 635, L29

Park C., Choi Y.-Y., Vogeley M. S., Gott J. R. I., Blanton M. R., 2007, ApJ, 658, 898

Pier J. R., Munn J. A., Hindsley R. B., Hennessy G. S., Kent S. M., Lupton R. H., Ivezić Ž., 2003, AJ, 125, 1559

Quintero A. D., Berlind A. A., Blanton M. R., Hogg D. W., 2005, preprint (astro-ph/0512004)

Quintero A. D., Berlind A. A., Blanton M., Hogg D. W., 2006, preprint (astro-ph/0611361)

Richards G. T., et al., 2002, AJ, 123, 2945

Sandage A., 2005, ARA&A, 43, 581

Sandage A., Tammann G. A., 1981, A revised Shapley-Ames Catalog of bright galaxies. Washington: Carnegie Institution, 1981, Preliminary version

Sérsic J. L., 1968, Atlas de galaxias australes. Cordoba, Argentina: Observatorio Astronomico, 1968

Smith J. A., et al., 2002, AJ, 123, 2121

Sorrentino G., Antonuccio-Delogu V., Rifatto A., 2006, A&A, 460, 673

Storrie-Lombardi M. C., Lahav O., Sodré L., Storrie-Lombardi L. J., 1992, MNRAS, 259, 8P

Stoughton C., et al., 2002, AJ, 123, 485

Strateva I., et al., 2001, AJ, 122, 1861

Strauss M. A., et al., 2002, AJ, 124, 1810

Tinker J. L., Conroy C., Norberg P., Patiri S. G., Weinberg D. H., Warren M. S., 2007, preprint (arXiv/0707.3445)

Tucker D. L., et al., 2006, Astronomische Nachrichten, 327, 821 van den Bergh S., 2007, preprint (arXiv/0706.3724)

Yamauchi C., et al., 2005, AJ, 130, 1545

York D. G., et al., 2000, AJ, 120, 1579